

Design of a polarization splitter for an ultra-broadband dual-core photonic crystal fiber

Yongtao Li(李永涛), Jiesong Deng(邓洁松), Zhen Yang(阳圳), Hui Zou(邹辉), and Yuzhou Ma(马玉周)
Citation: Chin. Phys. B, 2022, 31 (**5**): 054215. DOI: 10.1088/1674-1056/ac3a63
Journal homepage: http://cpb.iphy.ac.cn; http://iopscience.iop.org/cpb

What follows is a list of articles you may be interested in

Generation of mid-infrared supercontinuum by designing circular photonic crystal fiber

Ying Huang(黄颖), Hua Yang(杨华), and Yucheng Mao(毛雨澄)
Chin. Phys. B, 2022, 31 (**5**): 054211. DOI: 10.1088/1674-1056/ac272c

High sensitivity plasmonic temperature sensor based on a side-polished photonic crystal fiber

Zhigang Gao(高治刚), Xili Jing(井西利), Yundong Liu(刘云东), Hailiang Chen(陈海良), and Shuguang Li(李曙光)
Chin. Phys. B, 2022, 31 (**2**): 024207. DOI: 10.1088/1674-1056/ac0a63

Mid-infrared supercontinuum and optical frequency comb generations in a multimode tellurite photonic crystal fiber

Xu Han(韩旭), Ying Han(韩颖), Chao Mei(梅超), Jing-Zhao Guan(管景昭), Yan Wang(王彦), Lin Gong(龚琳), Jin-Hui Yuan(苑金辉), and Chong-Xiu Yu(余重秀)
Chin. Phys. B, 2021, 30 (**9**): 094207. DOI: 10.1088/1674-1056/abf10f

Generation of wideband tunable femtosecond laser based on nonlinear propagation of power-scaled mode-locked femtosecond laser pulses in photonic crystal fiber

Zhiguo Lv(吕志国) and Hao Teng(滕浩)
Chin. Phys. B, 2021, 30 (**4**): 044209. DOI: 10.1088/1674-1056/abe231

A compact electro-absorption modulator based on graphene photonic crystal fiber

Guangwei Fu(付广伟), Ying Wang(王颖), Bilin Wang(王碧霖), Kaili Yang(杨凯丽), Xiaoyu Wang(王晓愚), Xinghu Fu(付兴虎), Wa Jin(金娃), Weihong Bi(毕卫红)
Chin. Phys. B, 2020, 29 (**3**): 034209. DOI: 10.1088/1674-1056/ab6838

Design of a polarization splitter for an ultra-broadband dual-core photonic crystal fiber

Yongtao Li(李永涛)[1], Jiesong Deng(邓洁松)[2], Zhen Yang(阳圳)[2], Hui Zou(邹辉)[2,3,†], and Yuzhou Ma(马玉周)[4]

[1] *Academic Affairs Office, Nanjing University of Posts and Telecommunications, Nanjing* 210023, *China*
[2] *College of Electronic and Optical Engineering, Nanjing University of Posts and Telecommunications, Nanjing* 210023, *China*
[3] *State Key Laboratory of Luminescence and Applications, Changchun* 130033, *China*
[4] *Beijing Times Photoelectric Technology Co., Ltd, Beijing* 100094, *China*

(Received 28 July 2021; revised manuscript received 27 October 2021; accepted manuscript online 17 November 2021)

A novel ultra-broadband polarization splitter based on a dual-core photonic crystal fiber (DC-PCF) is designed. The full-vector finite element method and coupled-mode theory are employed to investigate the characteristics of the polarization splitter. According to the numerical results, a graphene-filled layer not only broadens the working bandwidth but also reduces the size of the polarization splitter. Furthermore, the fluorine-doped region and the germanium-doped region can broaden the bandwidth. Also, the 4.78 mm long polarization splitter can achieve an extinction ratio of −98.6 dB at a wavelength of 1550 nm. When extinction ratio is less than −20 dB, the range of the wavelength is 1027 nm–1723 nm with a bandwidth of 696 nm. Overall, the polarization splitter can be applied to all-optical network communication systems in the infrared and near-infrared wavelength range.

Keywords: photonic crystal fiber, polarization splitter, broadband bandwidth, extinction ratio

PACS: 42.81.Qb, 42.79.Fm, 42.68.Mj **DOI:** 10.1088/1674-1056/ac3a63

1. Introduction

A polarization splitter, as an important component in an all-optical network system, plays a significant role in optical fiber communication and optical fiber sensing.[1] Its main function is to decompose a beam of light into two mutually orthogonal polarized beams. However, a polarization splitter based on a traditional dual-core (DC) fiber is not conducive to device integration because the small birefringence of the traditional fiber leads to a long polarization splitter. In addition, a polarization splitter based on a traditional dual-core fiber has strong wavelength dependence and a narrow working band, which limits its application range.[4] Since photonic crystal fibers (PCFs) became available in 1996, they have attracted extensive attention from researchers due to their infinite single-mode transmission, high birefringence, flexible nonlinear and adjustable dispersion and other unique characteristics.[5] Through flexible adjustment of medium materials as well as the size and position of air holes in the inner and outer cladding, researchers can obtain a fiber suitable for different optical devices. This provides another direction for the design of new polarization splitters, which solves the problems of traditional polarization splitters, such as a poor splitting effect, a narrow working band and difficulties with integration.[10–18]

A polarization splitter based on a DC PCF has flexible and controllable structural parameters, and can easily realize various novel characteristics and overcome the disadvantages of traditional fiber splitters such as a narrow band and wavelength dependence. In 2003, Zhang and Yang[10] proposed a polarization splitter based on a DC PCF for the first time; they could obtain high birefringence by increasing or decreasing the diameter of different air holes in the cladding. Superior to the traditional polarization splitter, this splitter achieved a working bandwidth of 40 nm near 1550 nm on the premise that the extinction ratio is greater than 10 dB. At the same time, the advantages of a PCF for designing a polarization splitter were also highlighted. In 2005, Florous *et al.*[11] put forward a PCF with elliptical holes. The fiber was capable of splitting a beam at 1310 nm and 1550 nm. In 2006, Rosa *et al.*[12] designed a PCF polarization splitter arranged in a square lattice, with a length of 20 mm and a working bandwidth of 90 nm. In 2012, Liu *et al.*[13] put forward a novel kind of polarization splitter in a DC elliptical hole hybrid PCF. As shown by the numerical results, an extinction ratio of −64 dB was achieved at a wavelength of 1550 nm. A 1.92 mm long splitter was suggested to achieve a bandwidth of 150 nm with an extinction ratio better than −10 dB. Only by changing the structural parameters of the optical fiber can the maximum working bandwidth reach 150 nm. Nevertheless, most of the above beam splitters do not meet the technical requirements of simple construction: the size, shape and location of the air holes are difficult to accurately control during production.[14]

The refractive index of the core is reduced by doping fluorine in the core, and hence the refractive index difference between fiber cores increases, leading to an increase in coupling strength and a reduction in the size of the DC fiber. In 2004,

†Corresponding author. E-mail: zouhui1010@163.com

© 2022 Chinese Physical Society and IOP Publishing Ltd

this method was first introduced into the design of wideband polarization splitters.[15] Laegsgaard *et al.*[15] suggested expanding the bandwidth of DC fiber by adding fluorine to the fiber core. This DC PCF with a low refractive index core reduced the coupling length in the short-wave band. In 2013, Han *et al.*[16] designed a DC PCF polarization splitter with a fiber core doped with fluorine. Its length and bandwidth were 7.362 mm and 600 nm, respectively, when the extinction ratio was lower than −20 dB. In 2016, Zhao *et al.*[17] introduced a modulation core and two fluorine-doped cores to achieve an ultrawide bandwidth. According to their numerical results, an ultra-broadband splitter with a bandwidth of 320 nm could be achieved by using a 52.8 mm long PCF. Although the coupling length of a fiber core doped with fluorine tends to be flat with change in the wavelength, the mode fields of the two cores overlapped with the high doping concentration. In the design process, the refractive index of fluorine is difficult to control accurately.[13] Beyond that, this method cannot increase the coupling length ratio, and the polarization splitter must have a long length, which is not conducive to integrated applications.[18]

Recently, researchers have found that many properties of DC PCFs can be combined with the surface plasmon resonance (SPR) effect. When the incident light energy is propagated inside a DC PCF coated with a metal (or other dielectric material) on the central air hole, the free electrons on the metal (or other dielectric material) surface of the most central air hole will interact with the incident light energy to produce the SPR effect and excite the surface plasmon polariton (SPP) mode on the metal (or other dielectric material) surface. Thus, the resonant coupling strength of a DC PCF can be changed to achieve the phase matching condition at a certain wavelength, and the length of the splitter can be reduced. In 2014, Chen *et al.*[19] reported a novel polarization splitter based on a DC silica glass PCF with a liquid crystal modulation core. Apart from that, an anisotropic nematic liquid crystal (NLC) of E7 (material type) infiltrated into the central air hole leads to large birefringence, which makes splitters suffer a sharp increase in coupling length. The separate length was 0.175 mm and the extinction ratio −80.7 dB at the communication wavelength of 1550 nm. In 2016, Ma *et al.*[18] proposed a DC PCF splitter with graphene covering the central air hole; this had a bandwidth of up to 610 nm and an extinction ratio of 56.3 dB at 1550 nm. The SPP mode was generated between pure quartz and graphene upon the incidence of light. The light energy was coupled from the core to the graphene surface, leading to an increase in the effective refractive index difference. At the same time, the coupling length remained flat in a wide range and the bandwidth was broadened. In 2017, Bai and Wang[20] designed a DC PCF polarization splitter based on gold line filling. The length of the device was 0.263 mm, and the extinction ratio at 1550 nm and the bandwidth were −70 dB and 124 nm, respectively. In 2021, Qu *et al.*[21] investigated a DC PCF polarization beam splitter with a simple structure covering the E + S + C + L + U band based on the SPR effect. The total splitting bandwidth was 315 nm. By introducing gold line/film and other dielectric materials the plasma mode resonates with the core mode, thus enhancing the polarization characteristics of the fiber. In addition, the size of the splitter is also reduced.

In this paper, an ultra-wideband DC PCF polarization splitter based on fluorine/germanium doping and a graphene coating is proposed. Moreover, germanium is introduced to break the symmetry of the DC fiber to obtain higher mode birefringence and achieve stronger polarization characteristics. The coupling effect between the SPP mode on the surface of metal and graphene and the core mode is adopted to increase the difference in coupling length between the two polarization directions, which can be more favorable to the separation of polarization states. Moreover, this structure has a large fabrication tolerance. When the wavelength is 1550 nm, the spectral ratio can reach −98.6 dB. In the range of 1027 nm–1723 nm, the spectral ratio is less than −20 dB, resulting in a ultrawide working bandwidth of 696 nm, and the length of the beam splitter is only 4.78 mm. Compared with the known splitters of the same type, this splitter has better spectral efficiency. In addition, compared with the literature,[22] the operating bandwidth of this splitter is 78 nm wider. In short, it has great application prospects in future ultra-wideband, integrated and high-speed all-optical network systems.[18]

2. Structure and principle of the polarization splitter

2.1. Structure of the polarization splitter

Figure 1 shows the cross section of the DC PCF proposed in this paper. The fiber's substrate material is pure quartz and the air holes have a filled regular hexagon arrangement, with a diameter of d and a hole spacing of Λ. Fiber core region A is doped with fluorine, and region B is doped with germanium. The diameter of the central air hole is d_c. The outer layer is wrapped with a graphene thin wall, forming a ring structure. The thickness of the graphene ring is t, and $d_c = d - 2t$, as shown in Fig. 2.

The effective refractive index of the pure quartz substrate material is calculated by the Sellmeier formula[6]

$$n^2(\lambda) = 1 + \sum_{i=1}^{3} \frac{A_i \lambda^2}{\lambda^2 - \lambda_i^2}. \tag{1}$$

Here, $A_1 = 0.6961663$, $A_2 = 0.4079426$, $A_3 = 0.8974794$, $\lambda_1 = 0.0684043$ μm, $\lambda_2 = 0.1162414$ μm, and $\lambda_3 = 9.896161$ μm (λ is the wavelength). The absolute value of the difference between the refractive index of the fluorine-doped core and that of pure quartz is Δ_1. Beyond that, the

absolute value of the difference between the refractive index of the germanium-doped core and that of pure quartz is Δ_2. Meanwhile, Δ_1 and Δ_2 are related to the concentrations of fluoride and germanium.[16] The effective refractive index of graphene[23] is ($C_1 = 5.446\ \mu m^{-1}$)

$$n(\lambda) = 3 + i(C_1/3)\lambda. \tag{2}$$

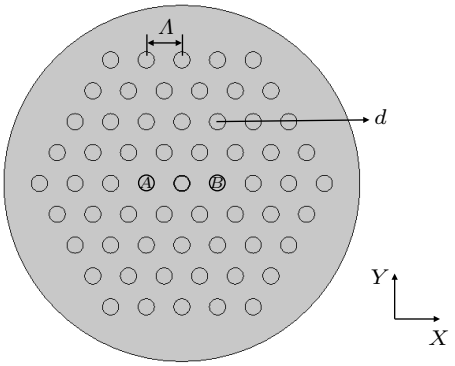


Fig. 1. Cross section of the DC PCF.

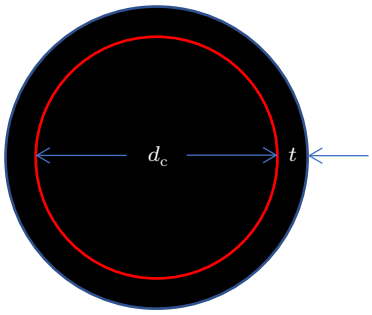


Fig. 2. Cross section of the central air hole.

2.2. Theoretical basis

According to mode-coupling theory, there are four super modes in a DC PCF: the odd mode and even mode in the direction of x-polarization, and the odd mode and even mode in the direction of y-polarization.[24] Since the odd and even modes of the same polarization state are coupled along the propagation direction of the fiber, the polarized light energy is transferred from one fiber core to another one. When the incident light energy of one polarization direction in the fiber core is 0, the corresponding propagation distance is called the coupling length L_c, which can be expressed as follows:[25]

$$L_c^{x,y} = \frac{\lambda}{2\left|n_{e,\lambda}^{x,y} - n_{o,\lambda}^{x,y}\right|}, \tag{3}$$

where $n_{e,\lambda}^{x,y}$ and $n_{o,\lambda}^{x,y}$ refer to the effective refractive index of the even and odd modes of x-polarization and y-polarization, respectively. They are calculated by the all-vector finite element method (FEM), with incident wavelength of λ. Due to the existence of double refraction L_c^x and L_c^y are unequal. To realize the full penny beam, the coupling length of x and y directions should be satisfied as[13]

$$L_c^y : L_c^x = \frac{\left|n_e^x - n_o^x\right|}{\left|n_e^y - n_o^y\right|} = m : n, \tag{4}$$

where m and n are integers with opposite evenness. As long as the fiber length, when the transmission distance of incident light in the fiber core is z, polarization beam splitting can be realized. At this point, the coupling length ratio is $\delta = L_c^y/L_c^x = m/n$. Obviously, m and n can have multiple sets of values. Given the microstructure and easy integration of devices, $m = 2$ and $n = 1$ are the best values.

It is assumed that the power of incident light into the core is P_{in}; then the power in x and y polarization directions at the output ends of cores A and B are respectively[13,20]

$$P_{out,A}^{x,y} = P_{in}\cos^2\left(\frac{\pi}{2}\cdot\frac{z}{L_c^{x,y}}\right), \tag{5}$$

$$P_{out,B}^{x,y} = P_{in}\sin^2\left(\frac{\pi}{2}\cdot\frac{z}{L_c^{x,y}}\right). \tag{6}$$

The extinction ratio (ER) indicates the crosstalk between x and y polarization states in the same fiber core, which is an important parameter for evaluating the performance of the polarization splitter. The extinction ratio of fiber cores A and B can be expressed as follows:[13,20,26]

$$ER_A = 10\log_{10}\left(\frac{P_{out,A}^y}{P_{out,A}^x}\right), \tag{7}$$

$$ER_B = 10\log_{10}\left(\frac{P_{out,B}^x}{P_{out,B}^y}\right). \tag{8}$$

3. Results and analysis

The object of research in this paper is PCF, and the research tool is COMSOL Multiphysics 5.6 simulation software. Meanwhile, the research method is the full vector FEM. The FEM provides high accuracy and flexible triangular meshes and is implemented to characterize the designed polarization splitter. Beyond that, the PCF is divided into 28376 triangular meshes. The number of mesh vertices is 14279 and the mesh area is $2.811 \times 10^{-10}\ m^2$. The scattering boundary condition is employed in the simulation process.[18]

The operating bandwidth and device size are two key parameters for evaluating the characteristics of the polarization splitters. Theoretically, the coupling length of the DC PCF (L_c), the coupling length ratio (δ) and the relative coupling length ratio (L_r) are closely related to these two indicators. The final structural parameters of the optical fiber are $d = 1\ \mu m$, $\Lambda = 2.2\ \mu m$, $t = 45.5$ nm, and $\Delta_1 = \Delta_2 = 0.0002$. In addition, the whole vector FEM is used for the research and analysis.

3.1. Coupling length and coupling ratio

The coupling length is an important parameter for measuring the coupling effect between two cores. With other conditions are unchanged, the shorter the coupling length, the stronger the coupling characteristics. As shown in Fig. 3(a), with or without graphene rings, the coupling length of x and y polarization directions L_c varies with wavelength. As displayed in Fig. 3(b), when the thickness of the graphene ring t changes, curves of the x and y polarization coupling length L_c vary with wavelength. Figures 4(a) and 4(b) reveal the curves of coupling length ratio varying with wavelength in the two cases.

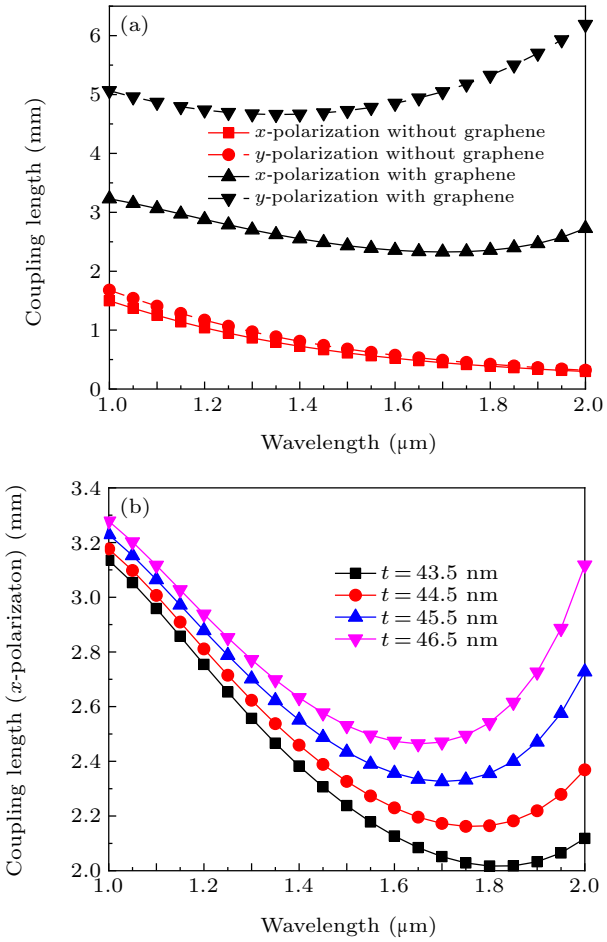


Fig. 3. Plots of coupling length versus wavelength: (a) PCF with or without graphene; (b) different thicknesses of graphene (x-polarization).

As shown in Figs. 3(a) and 4(a), although the coupling length of the graphene ring-free structure is short, the coupling length ratio remains around 1.1, leading to large values for m and n. However, this makes the device length longer. Apart from that, the addition of a graphene ring to the central air hole increases the coupling length, but the coupling length ratio also increases with increase in wavelength. The reason for this phenomenon is that there is an energetic coupling between the SPP patterns[27,28] generated by the inner walls of the graphene rings and the core patterns. Figure 5 displays the two-dimensional and three-dimensional mode field distributions of even modes in the y-polarization direction of fiber core at different wavelengths. In addition, the direction of the red arrows in the two-dimensional figure represents the direction of the electric field, and the density represents the magnitude of the electric field. It can be observed from the figure that the energy of the mode field is mainly concentrated in the two core regions at the beginning, but with increasing wavelength the energy is transferred from the core to the central air hole. At this time, the coupling effect between the core mode and the SPP mode becomes increasingly obvious. As revealed in Fig. 6, the mode field distribution of even modes in the x-polarization direction of the fiber core at different wavelengths is similar to that in the y-polarization direction. The difference is that the energy of the central air hole is concentrated on the graphene ring in the x-polarization direction. Figure 7 displays the distributions of odd-mode two-dimensional and three-dimensional mode fields of the fiber core in the y-polarization direction at different wavelengths. Obviously, at three different wavelengths there is no obvious energy coupling between the odd mode of the fiber core and the second-order graphene SPP mode. Besides, the energy of the mode field is concentrated in fiber cores A and B, and there is no strong interaction with the graphene layer.

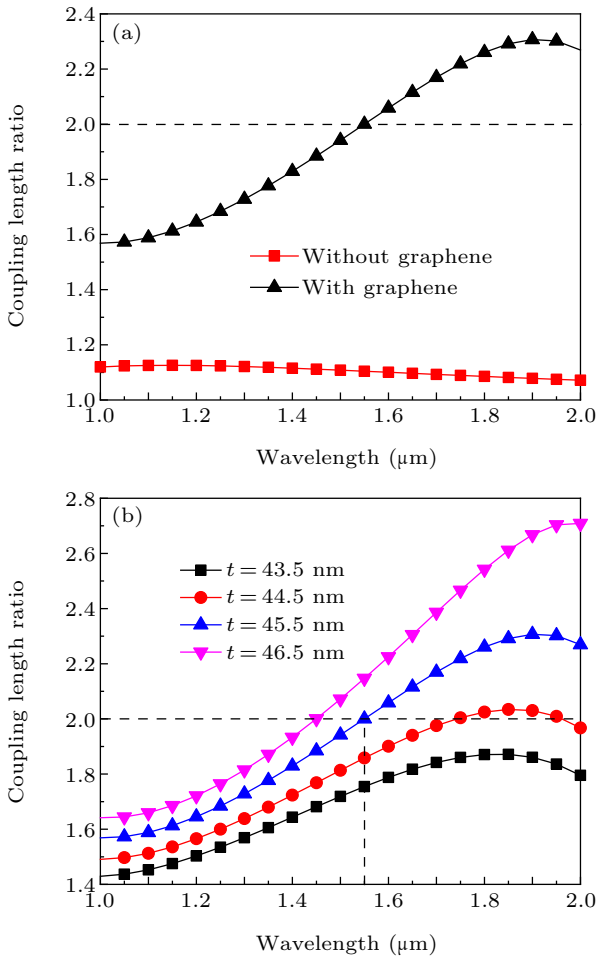


Fig. 4. Plots of coupling length ratio versus wavelength: (a) PCF with or without graphene; (b) different thicknesses of graphene.

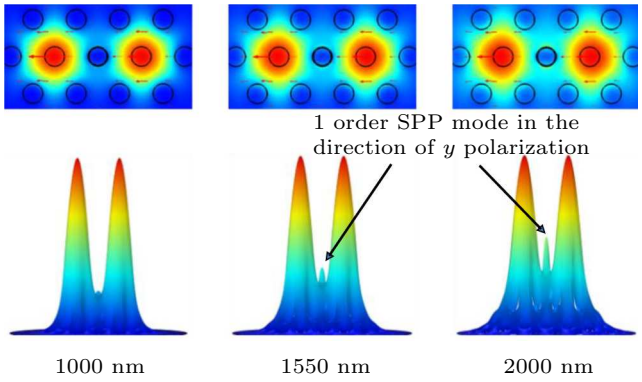


Fig. 5. Two- and three-dimensional electrical field distributions of the *y*-polarization even mode at different wavelengths.

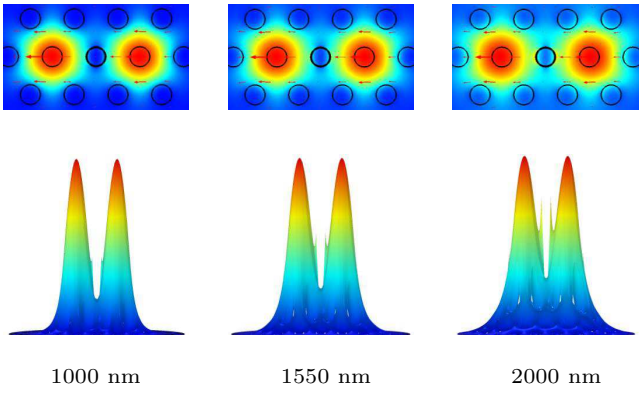


Fig. 6. Two- and three-dimensional electrical field distributions of the *x*-polarization even mode at different wavelengths.

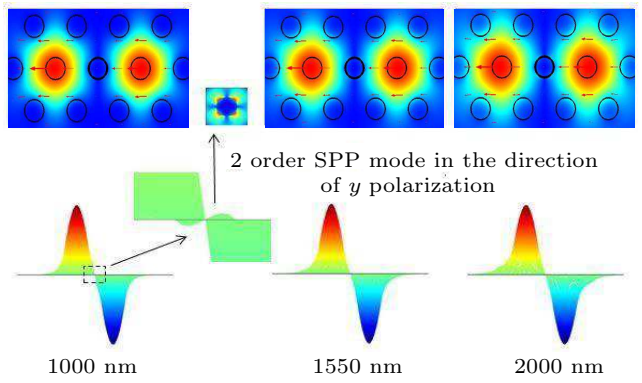


Fig. 7. Two- and three-dimensional electrical field distributions of the *y*-polarization odd mode at different wavelengths.

Under the same wavelength, the coupling difference between odd and even modes and SPP modes will affect the change in the effective refractive index of the modes, as shown in Fig. 8. As displayed in Fig. 8(b), the two effective refractive index curves are very close compared with the two cases of the fiber with and without a graphene ring structure. Namely, the odd-mode effective refractive index in the *y*-polarization direction has little numerical variation. As shown in Fig. 8(a), with increase in wavelength, the gap between the two curves becomes bigger. Apart from that, the even mode of the *y*-polarization direction is greatly influenced by the graphene SPP mode. As a result, the change in the even-mode effective refractive index of the *y*-polarization direction is greater than that of the odd-mode effective refractive index. Meanwhile, the two blue difference curves of amplitude changes in the figure reflect the differences more intuitively.

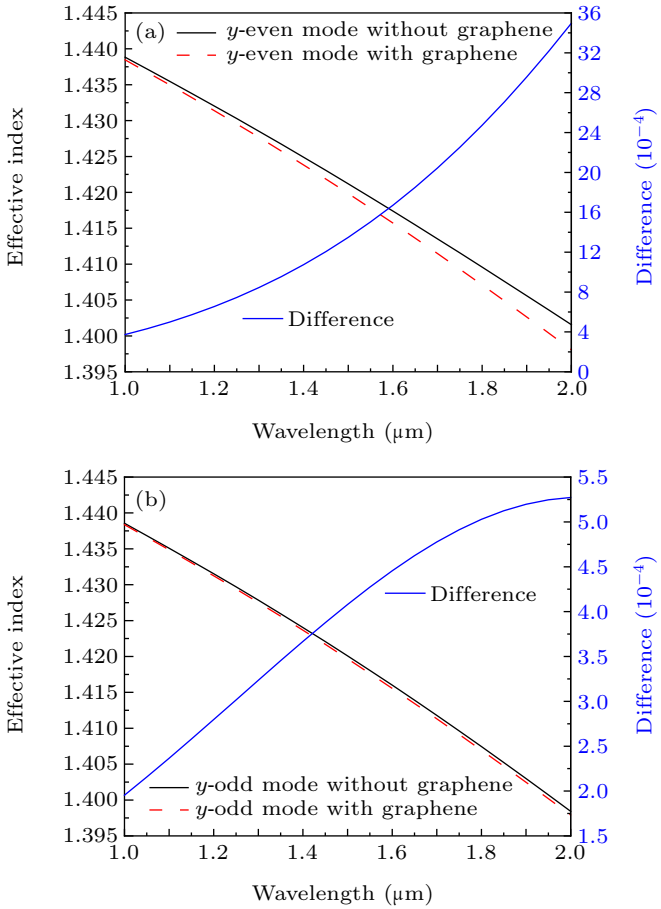


Fig. 8. Plots of effective index versus wavelength: (a) *y*-polarization even mode; (b) *y*-polarization odd mode.

As shown in Fig. 9, in the absence of a graphene ring structure, the effective refractive index difference of the *x*-direction (i.e., $|n^x_{e,\lambda} - n^x_{o,\lambda}|$) and *y*-direction (i.e., $|n^y_{e,\lambda} - n^y_{o,\lambda}|$) without graphene increase approximately exponentially, while those with a graphene ring structure increase parabolically. The growth rate of $|n^x_{e,\lambda} - n^x_{o,\lambda}|$ with a graphene ring structure is much greater than that of $|n^y_{e,\lambda} - n^y_{o,\lambda}|$. In the *x*-direction, the difference increases from 1.5483×10^{-4} to 3.85618×10^{-4} in the wavelength range from 1 μm to 1.87 μm. Nevertheless, the difference just increases from 0.9871×10^{-4} to 1.6914×10^{-4} in the wavelength range from 1 μm to 1.77 μm. This is further proof that graphene has a stronger influence on the *x*-direction coupling strength. With increase in wavelength, the difference between increases sharply. According to formula (4), when the difference in the effective refractive index increases, the coupling length ratio increases and the ideal ratio of 2:1 is easily achieved. Therefore, adding the graphene ring structure is more conducive to realizing the function of the splitter. As shown in Figs. 3(b) and 4(b), when the thickness of the graphene ring *t* increases, the coupling length and the coupling length ratio will increase accordingly. According to the

working wavelength, the best value of graphene ring thickness when the coupling length ratio is 2:1 is selected. Generally speaking, taking $\lambda = 1550$ nm, we could obtain the optimal value of the graphene thickness, $t = 45.5$ nm.

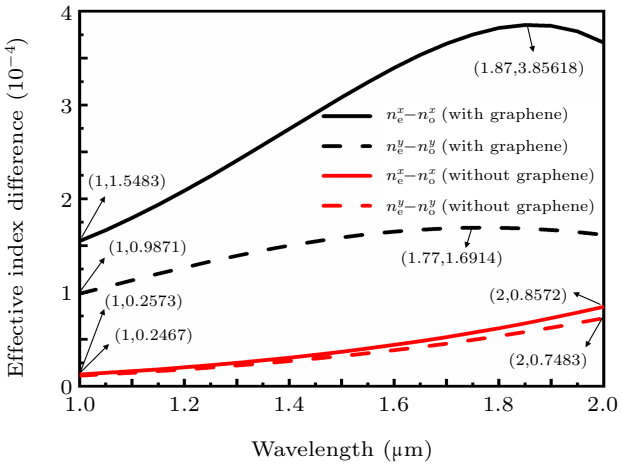


Fig. 9. Plots of effective refractive index difference versus wavelength.

3.2. Relative coupling length ratio

According to the results of the mathematical analysis, when λ_0 has a fixed value, the ratio of the coupling length of any wavelength λ to that of the working wavelength λ_0 should be close to 1. In this way, the polarization splitter can obtain a wider working bandwidth. In this paper, the relative coupling length ratio is introduced to describe the above ratio, and can be expressed as follows:

$$L_{\mathrm{r}}^{x,y} = L_{\mathrm{c},\lambda}^{x,y} : L_{\mathrm{c},\lambda_0}^{x,y}. \tag{9}$$

According to Ref. [16], a fiber core doped with fluorine can make the relative coupling length ratio approach 1. In this research, the fiber core is co-doped with fluorine and germanium, and the two core areas are only doped with fluorine on one side and germanium on the other side to destroy the symmetry of the DC fiber. This is conducive to obtaining higher-mode birefringence and thus enabling the fiber to obtain stronger polarization characteristics. As displayed in Figs. 10(a) and 10(b), the order of magnitude of mode birefringence for the undoped fiber is 10^{-6}, and the order of magnitude of mode birefringence is increased to 10^{-4} in the case of fluoride and germanium co-doping.

Figure 11 shows the curve of the relative coupling length ratio for the x-polarization direction with and without fluoride and germanium in the fiber core changing with the wavelength. It is obvious that the structure can make the relative coupling length ratio approach 1 and the curve tends to be more obvious below a wavelength of 1550 nm. In fact, when the concentration of fluorine and germanium in the fiber core is too high (i.e., when the values of Δ_1 and Δ_2 get larger), the mode fields of the two cores will be squeezed to the center and overlapped, making it difficult to separate polarized light in two directions at the end of the splitter. Therefore, the values of Δ_1 and Δ_2 should not be too high.

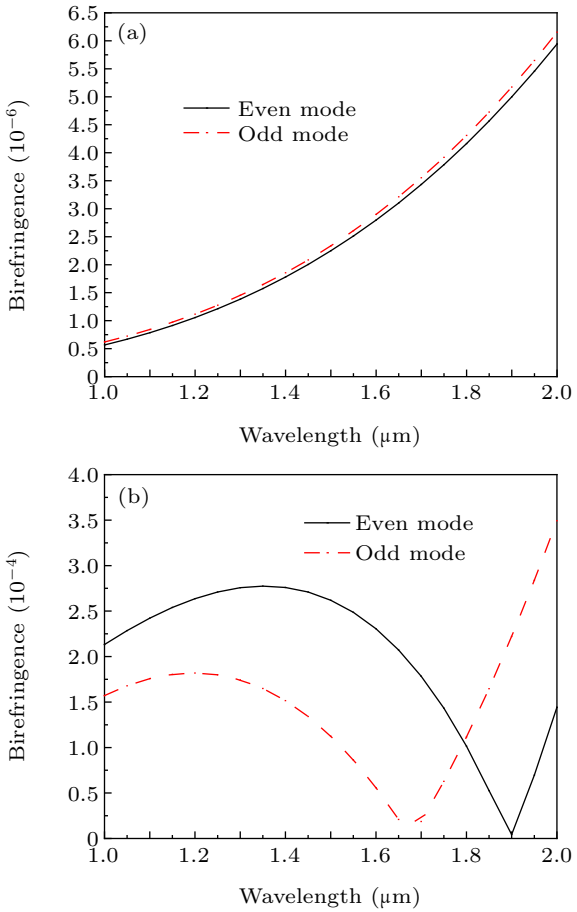


Fig. 10. Plots of birefringence versus wavelength: (a) without F and Ge; (b) with F and Ge.

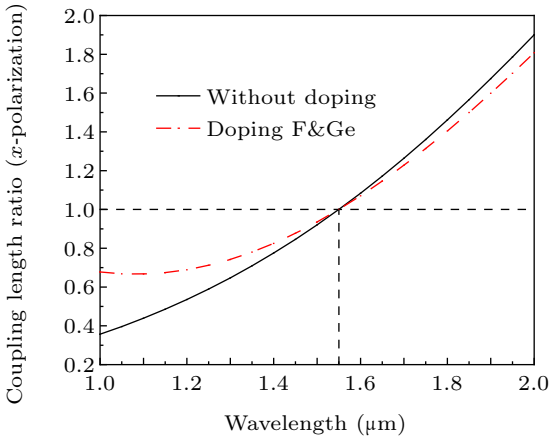


Fig. 11. Plots of relative coupling length ratio (x-polarization) versus wavelength.

3.3. Normalized power and extinction ratio

Figure 12 reveals that for wavelength $\lambda = 1550$ nm, the normalized power curve of a fiber core in the direction of x-polarization and y-polarization varies with the transmission distance. As shown in Fig. 12, when the beam is emitted into fiber core A, the energy in the direction of x-polarization and

y-polarization will undergo periodic transfer in fiber cores *A* and *B*. Under this wavelength, when the transmission distance $z = 2L_c^x = 2L_c^y = 4.78$ mm, the *x*-polarized light is in core *A* and the *y*-polarized light is coupled to core *B*, implementing the complete separation of the two polarization directions.

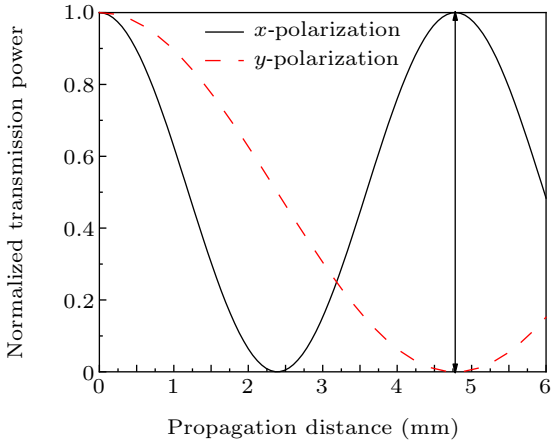


Fig. 12. Normalized power versus propagation distance.

The extinction ratio determines the effect of the polarization splitter. The larger the ratio is, the more favorable it is for the separation of the two polarization states. It is generally considered that the extinction ratio must be less than −20 dB to achieve the separation effect. Figure 13 shows the curve of extinction ratio versus wavelength when the transmission distance is 4.78 mm. It can be observed from Fig. 13 that at a wavelength of 1550 nm, the extinction ratio of cores *A* and *B* is −98.6 dB and −68.8 dB, respectively. At the same time, the wavelength range for an extinction ratio less than −20 dB is 696 nm and 432 nm, respectively. Table 1 compares the performance of the polarization splitter designed in this paper and those in other references. It is obvious that the polarization splitter designed in this paper has some advantages in terms of the extinction ratio and the working bandwidth.

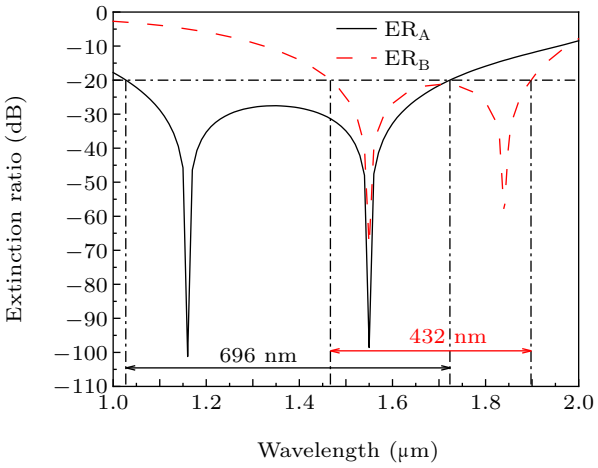


Fig. 13. Extinction ratio versus wavelength.

Table 1. Comparison of different polarization splitters.

Reference	Extinction ratio at 1550 nm (dB)	Working bandwidth (nm)	Working wavelength range (nm)
[2]	−25	400	1270–1670
[13]	−50.1	34	1533–1567
[16]	−46.6	600	1105–1705
[20]	−70	124	1482–1606
[22]	−132.92	618	1040–1658
[29]	−31	116	1481–1597
[30]	−53.46	120	1490–1610
Our work	−98.6	696	1027–1723

3.4. Confinement losses

Optical fiber communication is inseparable from loss, and the transmission over a certain distance is closely related to loss. Confinement loss, as an important index of fiber transmission, can be calculated using

$$L = 8.686 \times \frac{2\pi}{\lambda} \mathrm{Im}(n_{\mathrm{eff}}) \times 10^6. \tag{10}$$

The units of confinement loss and wavelength are dB/cm^{-1} and μm, respectively. In addition, Im(n_{eff}) refers to the imaginary part of the effective refractive index of the fundamental mode.

Figure 14 shows the confinement losses spectra of the four super modes. It can be seen that with increasing wavelength, the confinement of the energy in the transfer cores becomes weaker and the confinement losses get larger. Beyond that, the confinement loss of even modes in the *x*-polarization direction is the biggest. Notably, the loss of the *x*-polarization mode is greater than that of the *y*-polarization mode in the whole range, because two pores doped with fluorine and germanium are placed in the *x*-direction. Furthermore, the *x*-SPP mode is more easily coupled with the graphene ring than the *y*-SPP mode.[31]

3.5. Tolerance analysis

Given that the fiber is affected by external factors in the actual drawing process, the fiber structure parameters will show a certain deviation. Figure 15(a) displays the change of extinction ratio with wavelength when the fiber coupling length deviates from the initial coupling length by ±1%. As shown in the figure, a change of fiber coupling length of ±1% has little impact on the working bandwidth of the polarization

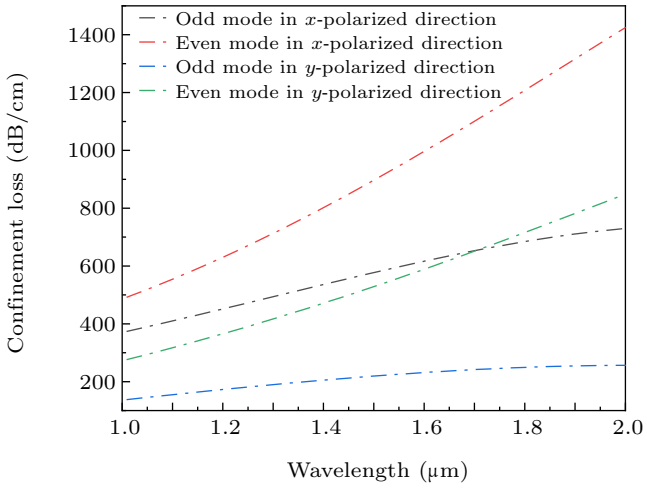


Fig. 14. The confinement losses spectra of the four super modes.

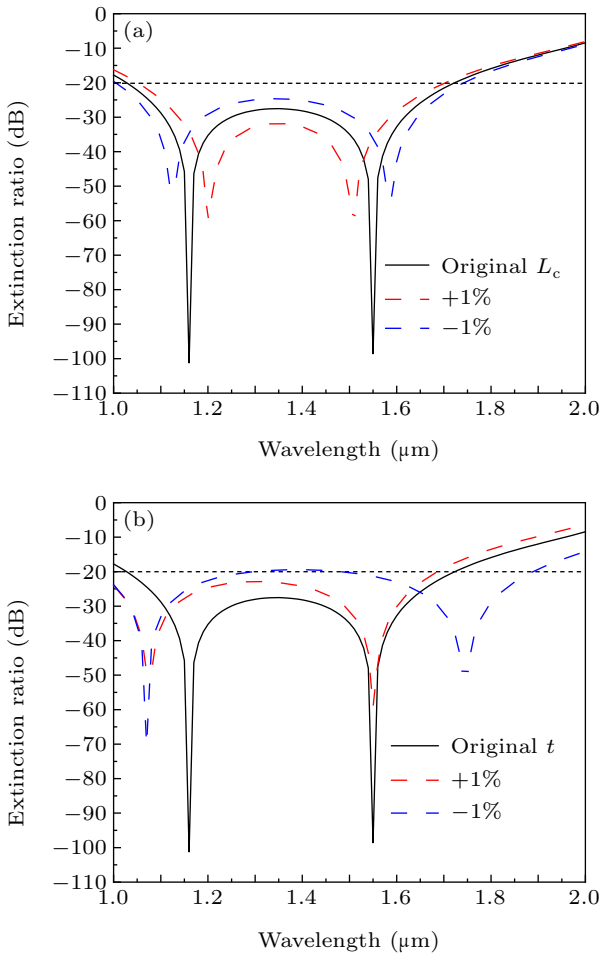


Fig. 15. Plots of extinction ratio versus wavelength: (a) coupling length ±1%; (b) thickness of graphene ±1%.

splitter, which is 650 nm and 730 nm, respectively. Figure 15(b) shows the change of extinction ratio with wavelength when the graphene ring thickness t deviates by ±1%. It can be observed from the figure that the bandwidth of the polarization splitter becomes 686 nm when t deviates by +1%. When the deviation of t is −1%, the bandwidth changes to 860 nm, and the curve of the extinction ratio moves up considerably. However, the extinction ratio is still around −20 dB, which has little impact on the polarization performance. Based on the above tolerance analysis, the fiber structure parameters changed by the external factors have little impact on the performance of the designed polarization splitter in the actual production process.

4. Conclusion

In this paper, a polarization splitter for an ultra-wideband, dual-core photonic crystal fiber was proposed. The optimal coupling length ratio of 2:1 and the relative coupling length ratio of nearly 1 were obtained by introducing a graphene ring and a fiber core doped with fluorine and germanium, which made the operating bandwidth of the polarization splitter wider and the device size smaller. According to simulation results, when the wavelength was 1550 nm, the extinction ratio could reach −98.6 dB. When the wavelength was between 1027 nm and 1723 nm (i.e., a bandwidth of 696 nm), the spectral ratio was less than −20 dB and the length of the beam splitter was 4.78 mm. Compared with the known splitters, the operating bandwidth of this splitter was nearly 100 nm wider, while the size of the device was reduced by a third. In addition, the structure had a certain production tolerance. When the coupling length or graphene thickness showed a numerical deviation of ±1%, good performance of the polarization splitter could be still guaranteed. Owing to the above excellent splitting characteristics, the proposed polarization splitter will be very important for applications in the field of ultra-wideband optical communications and integrated optics.

Acknowledgment

Project supported by the State Key Laboratory of Luminescence and Applications (Grant No. SKLA-2020-01).

References

[1] Florous N J, Saitoh K and Koshiba M 2006 *IEEE Photon. Technol. Lett.* **18** 1231
[2] Lu W L, Lou S Q, Wang X, Wang L W and Feng R J 2013 *Appl. Opt.* **52** 499
[3] Zhang X, Liao Q H, Chen S W, Hu P, Yu T B and Liu N H 2011 *Acta Phys. Sin.* **60** 104215 (in Chinese)
[4] Peng G D, Tjugiarto T and Chu P L 1990 *Electron. Lett.* **26** 682
[5] Knight J C, Birks T A, Russell P S J and De Sandro P D 1998 *Electron. Lett.* **34** 1347
[6] Roberts P J, Mangan B J and Sabert H 2005 *J. Opt. Fiber Commun. Res.* **2** 435
[7] Liao M, Yan X and Qin G 2009 *Opt. Express* **17** 15481
[8] Li W, Chen H and Chen M 2012 *Chin. J. Lasers* **39** 0205002
[9] Saitoh K, Koshiba M and Hasegawa T 2003 *Opt. Express* **11** 843
[10] Zhang L and Yang C X 2003 *Opt. Express* **11** 1015
[11] Florous N, Saitohk and Koshiba M 2005 *Opt. Express* **13** 7365
[12] Rosa L, Poli F, Foroni M, Cucinotta A and Selleri S 2006 *Opt. Lett.* **31** 441
[13] Liu S, Li S G and Zhu X P 2012 *Optik* **123** 1858
[14] Wang L W, Lou S Q, *et al.* 2012 *Chin. J. Lasers* **39** 126
[15] Laegsgaard Jesper, Bang Ole and Bjarklev Anders 2004 *Opt. Lett.* **29** 2473

[16] Han B L, Lou S Q, Lu W L, Su W, Zou H and Wang X 2013 *Acta Phys. Sin.* **62** 24 (in Chinese)
[17] Zhao T T, Lou S Q, Wang X, Zhou M and Lian Z G 2016 *Appl. Opt.* **55** 6428
[18] Ma Y 2016 *Optoelectron. Lett.* **12** 257
[19] Chen H L, Li S G, Fan Z K, *et al.* 2014 *IEEE Photon. J.* **6** 1
[20] Bai Y K and Wang B 2017 *Acta Photon. Sin.* **46** 7
[21] Qu Y, Yuan J, Qiu S, Zhou X, Li F, Yan B, Wu Q, Wang K, Sang X, Long K and Yu C 2021 *Sensors* **21** 496
[22] Tarek Rahman M and Abdul K 2019 *Appl. Opt.* **58** 9426
[23] Bao Q L 2011 *Nat. Photon.* **5** 411
[24] Ren G B, Wang Z, Jian S S and Lou S Q 2004 *Acta Phys. Sin.* **53** 2600 (in Chinese)
[25] Fan Z K, Li S G, Li J S, Wei Z Y and Tian W L 2015 *Opt. Mater.* **46** 384
[26] Jiang L H, Zheng Y, Hou L T, Zheng K, Peng J Y and Zhao X T 2015 *Opt. Commun.* **351** 50
[27] Dash J N and Jha R 2014 *IEEE Photon. Technol. Lett.* **26** 1092
[28] Maharana P K, Srivastava T and Jha R 2013 *IEEE Photon. Technol. Lett.* **25** 122
[29] Chen M Y, Sun B and Zhang Y K 2010 *Appl. Opt.* **49** 3042
[30] Guo S L, Huang H and Tong K 2014 *Infrared and Laser Engineering* **43** 1863
[31] Dou C, Jing X and Li S 2016 *Plasmonics* **11** 1163